DSMC Moving-Boundary Algorithms for Simulating MEMS Geometries with Opening and Closing Gaps

D. J. Rader, M. A. Gallis, and J. R. Torczynski

Engineering Sciences Center, Sandia National Laboratories, P. O. Box 5800, Albuquerque, NM 87185-0346, USA

Abstract. Moving-boundary algorithms for the Direct Simulation Monte Carlo (DSMC) method are investigated for a microbeam that moves toward and away from a parallel substrate. The simpler but analogous one-dimensional situation of a piston moving between two parallel walls is investigated using two moving-boundary algorithms. In the first, molecules are reflected rigorously from the moving piston by performing the reflections in the piston frame of reference. In the second, molecules are reflected approximately from the moving piston by moving the piston and subsequently moving all molecules and reflecting them from the moving piston at its new or old position.

Keywords: Direct Simulation Monte Carlo, MEMS, gas flow, moving boundary, noncontinuum
PACS: 47.45.-n, 47.61.Cb, 47.61.Fg, 47.45.Gx

INTRODUCTION

MicroElectroMechanical System (MEMS) devices typically have parts with micron-scale dimensions that move through air or other gases at atmospheric or reduced pressures. When a MEMS part moves toward or away from the adjacent substrate, the gas in the gap between the part and the substrate is compressed or expanded, respectively, which causes gas to flow out of the gap to the ambient environment or vice versa. This gas motion dissipates energy, so its effect on the dynamics of the MEMS part is called "squeeze-film damping" [1-5].

Since the mean free path is not negligible compared to MEMS geometric features, noncontinuum gas effects must be accurately treated. Many investigators have attempted to develop "compact" squeeze-film damping models compatible with ordinary-differential-equation MEMS dynamics models [6-10]. Although some experimental results exist [11-13], their limited precision often precludes development or assessment of such models.

The Direct Simulation Monte Carlo (DSMC) method of Bird [14-15] is capable of simulating noncontinuum gas flows to high accuracy. However, DSMC simulations have generally considered fixed geometries, whereas many MEMS systems have moving geometries. Here, a microbeam oscillating in an out-of-plane fashion near the substrate is considered, and DSMC moving-boundary algorithms are investigated for the analogous but simpler geometry of a piston oscillating between two parallel walls (see Figure 1).

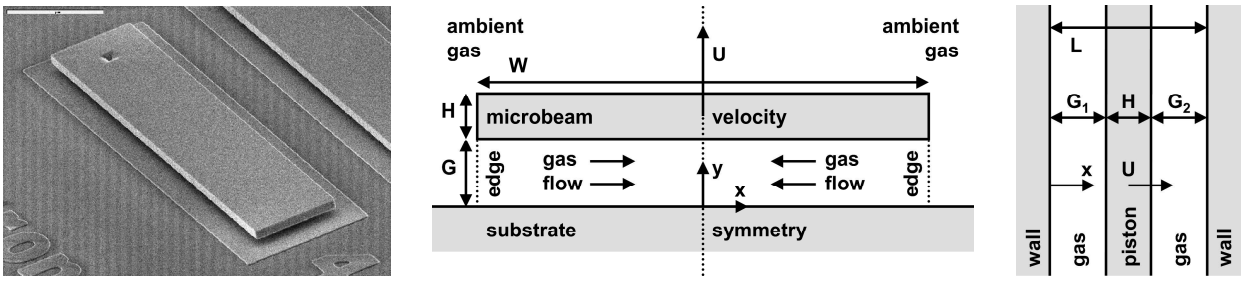

FIGURE 1. Left: Oscillating microbeam anchored at dimple. Middle: Microbeam cross section. Right: Piston geometry.

MOVING-BOUNDARY DSMC ALGORITHMS

Two moving-boundary DSMC algorithms are investigated in the context of the one-dimensional piston problem described in the previous section. The domain extends from $x = 0$ to $x = L$, and the piston has thickness H in the x direction (see Figure 1). This domain is spanned by N_x uniform cells of length $\Delta x = L/N_x$. Uniform cells are not required by the algorithms but are chosen for convenience. Although presented in a one-dimensional context, many aspects of these algorithms can be generalized to multi-dimensional flows, especially if the object executes rigid-body translational motion (i.e., all points on the body surface move with the same velocity vector at each time).

In both algorithms, the mesh is taken to be fixed throughout time, and the object moves over the mesh cells. More specifically, the mesh is not attached to the moving object and does not move or deform based on the object. Over the time interval from t to $t + \Delta t$, the object has a constant velocity U in the x direction, and the molecules have constant velocities u_i, v_i, and w_i in the x, y, and z directions, respectively. At time t, the object surfaces are at positions X_1 and X_2, and the molecules are at positions x_i such that all molecules lie outside the object (i.e., molecules do not overlap the object): either $x_i < X_1$ or $x_i > X_2$. The object and the molecules move for a time Δt, and their new positions are $\tilde{X}_j = X_j + U\Delta t$ and $\tilde{x}_i = x_i + u_i\Delta t$. If a molecule satisfies the same test that it satisfied prior to moving (i.e., either $\tilde{x}_i < \tilde{X}_1$ if $x_i < X_1$, or $\tilde{x}_i > \tilde{X}_2$ if $x_i > X_2$), then the molecule remained outside the object while moving during the entire time interval, and no reflection needs to be performed. However, if a molecule fails the same test that it satisfied prior to moving (i.e., either $\tilde{x}_i \geq \tilde{X}_1$ if $x_i < X_1$, or $\tilde{x}_i \leq \tilde{X}_2$ if $x_i > X_2$), then the molecule crossed the corresponding surface of the object while moving, and a reflection needs to be performed.

Figure 2 shows the two algorithms used to perform reflections. The first algorithm performs reflections in a rigorous manner. The object and molecule velocities are transformed into the object reference frame by subtracting the object velocity from the molecule velocity: $\Delta u_i = u_i - U$, $\Delta v_i = v_i$, $\Delta w_i = w_i$. A standard DSMC reflection [14] (e.g., a linear combination of diffuse fully accommodating and specular reflections) is performed to yield reflected velocities in the object reference frame: $\Delta\tilde{u}_i$, $\Delta\tilde{v}_i$, $\Delta\tilde{w}_i$. These velocities are subsequently transformed back to the mesh reference frame: $\tilde{u}_i = \Delta\tilde{u}_i + U$, $\tilde{v}_i = \Delta\tilde{v}_i$, $\tilde{w}_i = \Delta\tilde{w}_i$. The molecule is then moved at the reflected velocity for the remainder of the time step. The second algorithm performs reflections in an approximate manner. The principal difference between the approximate and the rigorous algorithms is that the approximate algorithm performs reflections with the object surface at its new position at time $t + \Delta t$ (i.e., at $\tilde{X}_1$ or $\tilde{X}_2$) if the surface is advancing into the gas or at its old position at time t (i.e., at X_1 or X_2) if the surface is receding from the gas, rather than at the exact reflection position. Since the exact positions at which reflections occur do not have to be determined, the approximate algorithm is faster. The approximate algorithm is correct in the limit that the object velocity is much smaller than the typical molecule velocity. This condition is often satisfied for MEMS devices in ambient air since MEMS components typically have speeds well below the speeds of air molecules (~300 m/s) [8].

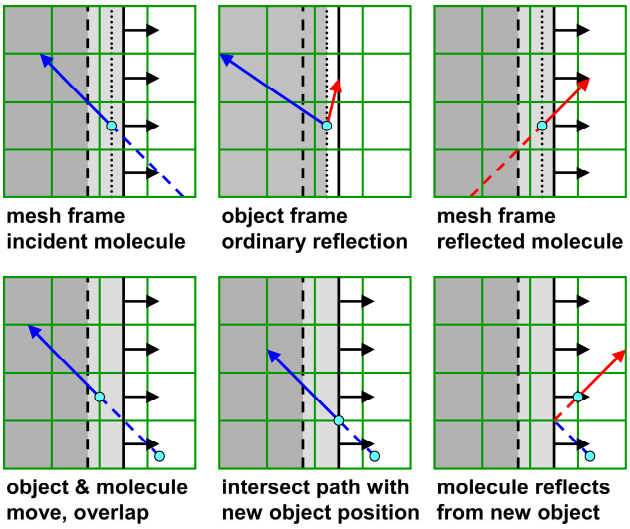

FIGURE 2. Fixed-mesh moving-boundary algorithms: top, rigorous; bottom, approximate with an advancing surface. Dashed lines: surface at start of time step. Solid lines: surface at end of time step. Dotted lines: exact reflection location.

MOVING-PISTON DSMC SIMULATIONS

Simulations using the rigorous and approximate fixed-mesh moving-boundary DSMC algorithms are performed for the moving-piston situation shown in Figure 1. Two types of piston motion are considered. In the first, the piston starts impulsively from rest, moves a prescribed distance at constant velocity, and then halts at this location. In the second, the piston oscillates sinusoidally about its initial position at a prescribed frequency.

The following conditions are common to all simulations. For verification purposes [16], the gas is taken to have the properties of argon in Bird [14] except that the molecules undergo hard-sphere collisions. The molecular mass is $m = 66.3\times10^{-27}$ kg, the viscosity temperature exponent is $\omega = 1/2$, the angular scattering exponent is $\alpha = 1$, the reference temperature is $T_{\text{ref}} = 273.15$ K, the reference viscosity at this temperature is $\mu_{\text{ref}} = 2.117\times10^{-5}$ Pa·s, the ratio of the infinite-to-first-approximation viscosities is $\mu_\infty/\mu_1 = 1.016034$, and the Boltzmann constant is $k_B = 1.380658\times10^{-23}$ J/K, which together yield the viscosity and the hard-sphere diameter [14,16]:

$$\frac{\mu}{\mu_{\text{ref}}} = \left(\frac{T}{T_{\text{ref}}}\right)^{\omega},\ d_{\text{ref}} = \left\{\frac{5(\alpha+1)(\alpha+2)}{4\alpha(5-2\omega)(7-2\omega)\mu_{\text{ref}}}\left(\frac{\mu_\infty}{\mu_1}\right)\left(\frac{mk_BT_{\text{ref}}}{\pi}\right)^{1/2}\right\}^{1/2}. \tag{1}$$

Initially, the gas is motionless and at pressure $p_{\text{init}} = 266.644$ Pa and temperature $T_{\text{init}} = 273.15$ K, which yield a number density of $n_{\text{init}} = p_{\text{init}}/k_BT_{\text{init}} = 7.0704\times10^{22}$ m^{-3}, a density of $\rho_{\text{init}} = mn_{\text{init}} = 4.6877\times10^{-3}$ kg/m^3, a mean molecular speed of $c_{\text{init}} = (8k_BT_{\text{init}}/\pi m)^{1/2} = 380.59$ m/s, and a mean free path of $\lambda_{\text{init}} = 2\mu_{\text{init}}/\rho_{\text{init}}c_{\text{init}} = 23.732$ μm.

The gas is confined between two parallel walls located at $x = 0$ and $x = L$, where the wall separation is $L = 1000$ μm, the wall temperatures are $T_{\text{wall}} = 273.15$ K, and the wall accommodation coefficients are $\sigma_{\text{wall}} = 1$. This domain is divided into $N_x = 100$ uniform cells of length $\Delta x = L/N_x = 10$ μm. Each of the cells not initially occupied by the piston is filled initially with $N = 10^5$ computational molecules. A time step of $\Delta t = 10^{-9}$ s is used, and an averaging time of $t_{\text{avg}} = \Delta t$ is used when field variables are output (i.e., only one time plane is "averaged"). These values yield normalized cell-size and time-step values of $\Delta x/\lambda_{\text{init}} = 0.42$ and $c_{\text{init}}\Delta t/\lambda_{\text{init}} = 0.016$, respectively, which indicate well resolved simulations.

The piston has a thickness $H = 2\Delta x = 20$ μm and is centered at $X[0] = L/2 = 500$ μm initially. Its two surfaces are located at $X_1[0] = X[0] - \Delta x = 490$ μm and $X_2[0] = X[0] + \Delta x = 510$ μm initially. The piston surface is at temperature $T_{\text{piston}} = 273.15$ K and has accommodation coefficient $\sigma_{\text{piston}} = 0$ or 1 (either specular or diffuse fully accommodating). The piston center position $X[t]$ is prescribed for all time, and the piston surface positions $X_{1,2}[t]$ and the piecewise-constant piston velocity $U[t \leftrightarrow t+\Delta t]$ averaged from time t to time $t+\Delta t$ (used when performing molecular reflections) are given in terms of the piston center position:

$$X_1[t] = X[t] - \Delta x,\ X_2[t] = X[t] + \Delta x,\ U[t \leftrightarrow t+\Delta t] = \big(X[t+\Delta t] - X[t]\big)/\Delta t. \tag{2}$$

The impulsively started piston has the following piston center position for all time $t \ge 0$:

$$X[t] = \min\big[X[0] + U_s \max[t,0], X_s\big],\ U_s = \{10,100\}\ \text{m/s},\ X_s = 0.75L = 750\ \mu\text{m}. \tag{3}$$

The piston thus starts at 50% across the domain, moves with constant velocity, and stops at 75% across the domain.

The oscillating piston has the following piston center position for all time $t \ge 0$:

$$X[t] = X[0] + X_0\sin[2\pi f_0 t],\ f_0 = 1\ \text{MHz},\ t_0 = 1/f_0 = 1\ \mu\text{s},\ U_0 = \{10,100\}\ \text{m/s},\ X_0 = U_0/(2\pi f_0). \tag{4}$$

These two velocity amplitudes yield corresponding displacement amplitudes of $X_0 = \{1.59,15.9\}$ μm, so $X_0/\Delta x = \{0.159,1.59\}$ cells are crossed during each quarter-cycle. Quantities are output 20 times per cycle.

Simulations terminate at 100 μs, by which time the gas on both sides of the piston is uniform and motionless. The results of the impulsive-piston and oscillating-piston simulations are shown in Figures 3 and 4, respectively. Here, velocity values of 100 m/s are referred to as "fast", and velocity values of 10 m/s are referred to as "slow".

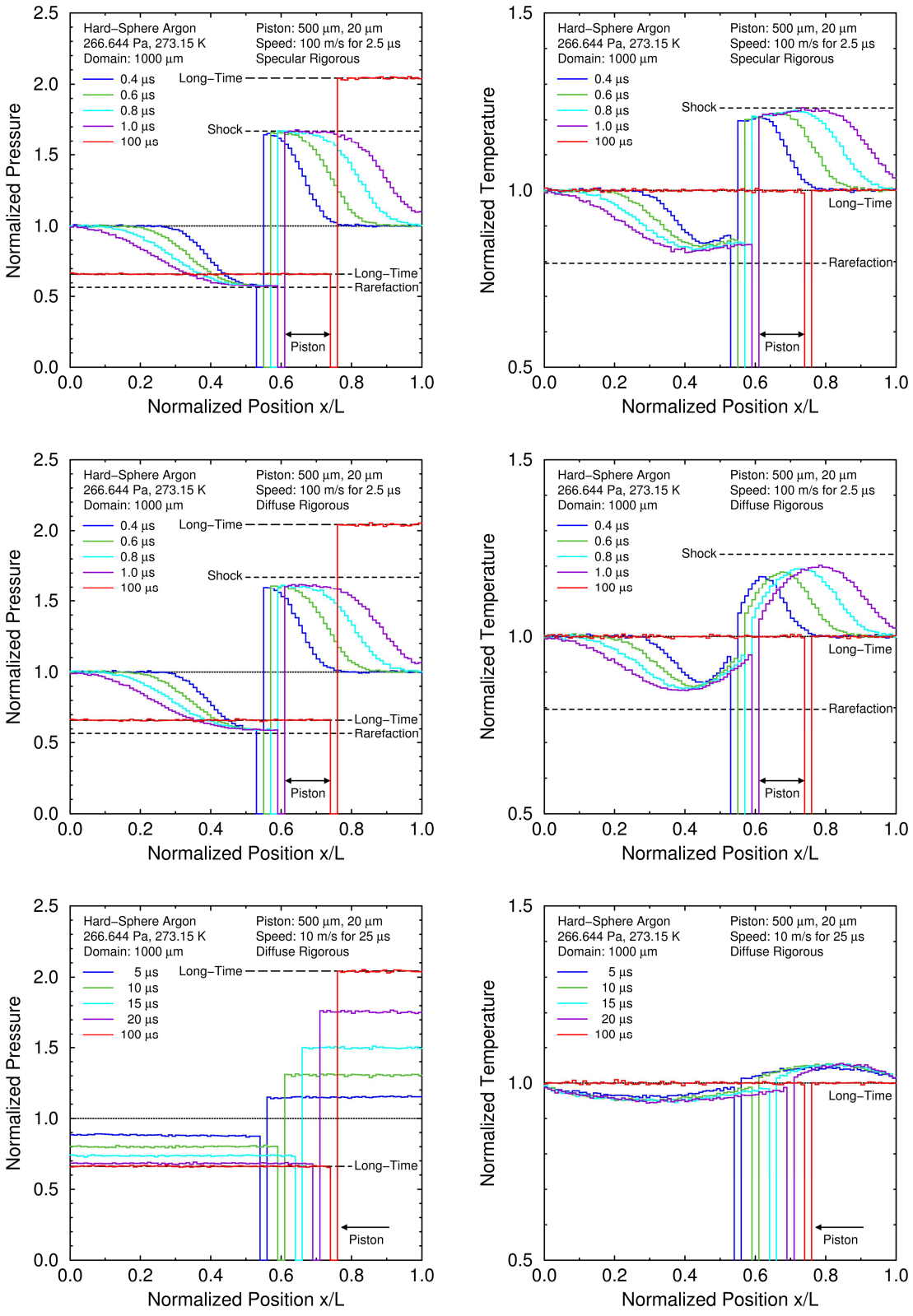

FIGURE 3. Pressure and temperature profiles for the impulsively started piston at indicated conditions.

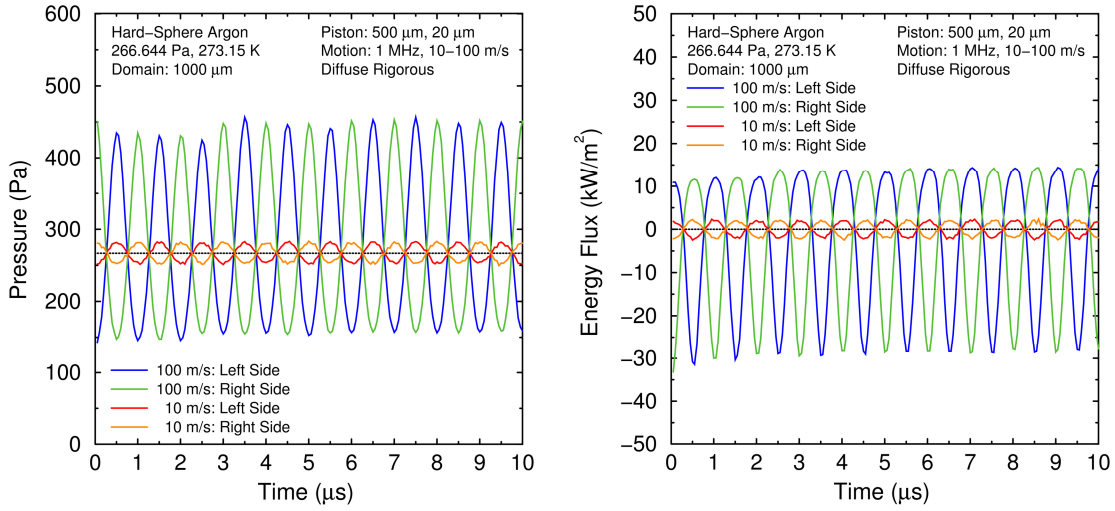

FIGURE 4. Pressure and energy-flux histories on both piston surfaces for the oscillating piston.

Figure 3 shows pressure and temperature profiles at selected times produced by the impulsively started piston for the fast and slow velocities. The profiles produced by the rigorous and approximate algorithms are essentially the same except for stochastic noise, so only the profiles from the rigorous algorithm are shown. Three combinations of velocity and accommodation coefficient are shown in this figure: the fast specular piston, the fast diffuse piston, and the slow diffuse piston. Although not identical, the profiles from the slow diffuse and specular pistons are qualitatively similar, so the latter profiles are not shown.

In the fast cases, a shock wave is generated by the advancing piston surface, and a rarefaction wave is generated by the receding piston surface. Initially, these two waves emerge from the Knudsen layers adjacent to the piston surfaces, which have thicknesses comparable to the shock thickness (here, ~10 mean free paths). Subsequently, the pressure and temperature jumps across these two waves approach their corresponding theoretical values [17]. Since each half of the domain is only about 20 mean free paths long at first, these waves are only marginally developed before they reach the Knudsen layers adjacent to the end walls of the domain and are subsequently reflected. In the shock wave, the temperature front slightly precedes the pressure front, as expected [14].

Although the gas temperatures adjacent to the fast specular piston are close to the shock and rarefaction values, the gas temperatures adjacent to the fast diffuse piston are close to the piston temperature. The thermal boundary layers produced in the gas by the diffuse piston weaken both waves. At long times relative to the piston stopping time (100 μs vs. 2.5 μs), the gas comes to rest with uniform temperature at the wall temperature and uniform pressures at the pressures corresponding to this temperature and the new volumes (i.e., normalized pressures of $49/74 \approx 0.662$ for the rarefaction side and $49/24 \approx 2.042$ for the shock side).

In the slow case, the waves generated from the piston surface are very weak, so the pressure is nearly uniform while the piston is moving (0-25 μs) and after the piston has stopped (after 25 μs). The temperature is slightly above the initial/wall value on the compression side and is slightly below the initial/wall value on the expansion side while the piston is moving. At long times, the pressure and temperature distributions are the same as for the fast cases because the piston undergoes the same total displacement in all cases.

Figure 4 shows pressure and energy-flux histories on both surfaces for the fast and slow oscillating pistons. As for the impulsive piston, the histories produced by the rigorous and approximate algorithms are essentially the same except for stochastic noise, so only the histories from the rigorous algorithm are shown. Also as above, the histories from the specular piston are not shown because they are qualitatively similar to the corresponding histories from the diffuse piston. This similarity applies not only to the pressure histories but also to the energy-flux histories because the latter are dominated by pressure-velocity power rather than by heat conduction. The slow cases produce linear waves, so their histories are essentially symmetric about the average values. The fast cases produce nonlinear waves, so the half-cycles of the histories associated with advancing or receding surfaces differ significantly and are not symmetric about the average values. In particular, averaging the total energy flux to the piston over one full cycle yields a negative value, which indicates that energy must be continually input to the piston to sustain the oscillation.

CONCLUSIONS

Moving-boundary algorithms for the Direct Simulation Monte Carlo (DSMC) method of molecular gas dynamics have been investigated. The motivation for this effort involves simulation of gas flows in opening and closing gaps for MEMS (MicroElectroMechanical Systems) devices in air. Two algorithms have been investigated: a rigorous algorithm, in which computational molecules are reflected from the exact points at which their trajectories intersect the moving object, and an approximate algorithm, in which computational molecules are reflected from the envelope formed by the object as it moves over one time step. The results from these algorithms agree closely when the object velocity is modest with respect to molecular velocities. Future efforts will focus on developing and implementing two-dimensional algorithms corresponding to the one-dimensional algorithms that are investigated here.

All of the examples presented here use a large number of molecules per cell to ensure that the profiles and histories from the simulations have extremely low noise relative to the signals of interest for verification purposes. However, the goal in many applications is to determine the gas force on an oscillating MEMS device and the power required to sustain its motion (or, correspondingly, the rate at which its motion decays). In this situation, the number of molecules per cell and the total number of molecules in a simulation can be reduced by orders of magnitude, and, when required, noise reduction can be achieved by averaging over many cycles or by ensemble averaging.

ACKNOWLEDGMENTS

Sandia National Laboratories is a multi-program laboratory operated by Sandia Corporation, a wholly owned subsidiary of Lockheed Martin Corporation, for the U.S. Department of Energy's National Nuclear Security Administration under contract DE-AC04-94AL85000.

REFERENCES

1. T.-R. Hsu, *MEMS & Microsystems: Design and Manufacture*, Boston: McGraw-Hill, 2002.
2. J. A. Pelesko and D. H. Bernstein, *Modeling MEMS and NEMS*, Boca Raton: Chapman & Hall/CRC, 2003.
3. J. J. Allen, *Micro Electro Mechanical System Design*, Boca Raton: Taylor & Francis, 2005.
4. G. Karniadakis, A. Beskok, and N. Aluru, *Microflows and Nanoflows: Fundamentals and Simulation*, New York: Springer, 2005.
5. M. Gad-el-Hak, *MEMS: Introduction and Fundamentals*, 2nd edition, Boca Raton: Taylor & Francis, 2006.
6. M. A. Gallis and J. R. Torczynski, "Simulation of Moving Microbeams with the Direct Simulation Monte Carlo Method," AIAA-2003-4013, Washington: American Institute of Aeronautics and Astronautics, 2003.
7. T. Veijola, "Compact Models for Squeezed-Film Dampers with Inertial and Rarefied Gas Effects," *Journal of Micromechanics and Microengineering*, **14**, 1109-1118 (2004).
8. M. A. Gallis and J. R. Torczynski, "An Improved Reynolds-Equation Model for Gas Damping of Microbeam Motion," *Journal of Microelectromechanical Systems*, **13**, (4), 653-659 (2004).
9. A. A. Alexeenko, E. P. Muntz, M. A. Gallis, and J. R. Torczynski, "Comparison of Kinetic Models for Gas Damping of Moving Microbeams," AIAA-2006-3715, Washington, DC: American Institute of Aeronautics and Astronautics, 2006.
10. X. Guo and A. Alexeenko, "Compact Model of Squeeze-Film Damping Based on Rarefied Flow Simulations," *Journal of Micromechanics and Microengineering*, **19**, 045026 (2009).
11. H. Sumali and D. S. Epp, "Squeeze Film Damping Models Compared with Tests on Microsystems," IMECE2006-14388, New York: American Society of Mechanical Engineers, 2006.
12. H. Sumali, D. S. Epp, J. R. Torczynski, and M. A. Gallis, "Experimental Validation of a Squeeze-Film Damping Model Based on the Direct Simulation Monte Carlo Method," DETC2007-34866, New York: American Society of Mechanical Engineers, 2007.
13. H. Sumali, "Squeeze-Film Damping in the Free Molecular Regime: Model Validation and Measurement on a MEMS," *Journal of Micromechanics and Microengineering*, **17**, 2231-2240 (2007).
14. G. A. Bird, *Molecular Gas Dynamics and the Direct Simulation of Gas Flows*, Oxford: Clarendon, 1994.
15. T. J. Bartel, S. J. Plimpton, and M. A. Gallis, "Icarus: A 2-D Direct Simulation Monte Carlo (DSMC) Code for Multi-Processor Computers, User's Manual – v 10.0," SAND2001-2901, Albuquerque: Sandia National Laboratories, 2001.
16. M. A. Gallis, J. R. Torczynski, D. J. Rader, M. Tij, and A. Santos, "Normal Solutions of the Boltzmann Equation for Highly Nonequilibrium Fourier Flow and Couette Flow," *Physics of Fluids*, **18**, 017104 (2006).
17. P. A. Thompson, *Compressible-Fluid Dynamics*, New York: McGraw-Hill Book Company, 1972.